polymers

MDPI

Article

Green, Eco-Friendly, Highly Biocompatible and Bioactive Nanocomposite-Based Biopolymers Loaded with ZnO@Fe_3O_4 Nanoparticles

Ayed S. Allogmani [1,*], Roushdy M. Mohamed [1,*] and Mohamed S. Hasanin [2,*]

[1] University of Jeddah, College of Science and Arts at Khulis, Department of Biology, Jeddah, Saudi Arabia
[2] Cellulose and Paper Department, National Research Centre, Dokki, Cairo 12622, Egypt
* Correspondence: asallogmani@uj.edu.sa (A.S.A.); mroushdy@uj.edu.sa (R.M.M.); sido_sci@yahoo.com (M.S.H.)

Abstract: Biocompatibility is a major concern for promising multifunctional bioactive materials. Unfortunately, bioactive materials lack biocompatibility in some respects, so active ingredient formulations are urgently needed. Bimetallic nanoparticles have demonstrated drawbacks in stabilized biocompatible formulations. This study examined the preparation of biomaterial-based multifunctional biopolymers via an eco-friendly formulation method using ultrasound. Bimetallic zinc oxide/iron oxide (magnetic form) nanoparticles (ZnO@Fe_3O_4NPs) were formulated using casein and starch as capping agents and stabilizers. The formulated nanocomposite was characterized using ultraviolet–visible spectroscopy (UV-vis), Fourier-transform infrared spectroscopy (FTIR), X-ray diffraction (XRD), thermal gravimetric analysis (TGA), scanning electron microscopy (SEM), and high-resolution transmission electron microscopy (HR-TEM). Herein, the formulated nanocomposite was shown to have a thermally stable nanostructure, and the bimetallic ZnO@Fe_3O_4 NPs were measured as 85 nm length and 13 nm width. Additionally, the biocompatibility test showed its excellent cytocompatibility with Wi 38 and Vero normal cell lines, with IC_{50} 550 and 650 mg/mL, respectively. Moreover, the antimicrobial activity was noted against six pathogens that are represent to the most common pathogenic microbes, with the time required for killing of bacteria and unicellular fungi being 19 h and 61 h for filamentous fungi with remarket an excellent antioxidant activity.

Keywords: nanocomposite; bimetallic; biocompatibility; antimicrobial activity; cytotoxicity activity

Citation: Allogmani, A.S.; Mohamed, R.M.; Hasanin, M.S. Green, Eco-Friendly, Highly Biocompatible and Bioactive Nanocomposite-Based Biopolymers Loaded with ZnO@Fe_3O_4 Nanoparticles. *Polymers* **2023**, *15*, 3641. https://doi.org/10.3390/polym15173641

Academic Editors: José Miguel Ferri and Vicent Fombuena Borràs

Received: 9 August 2023
Revised: 27 August 2023
Accepted: 30 August 2023
Published: 4 September 2023

1. Introduction

Microbial infections are defined as the invasion of tissues by pathogens, and the host tissues respond to the infectious agent that sometimes produces toxins that are released into surrounding areas [1,2]. Furthermore, a sickness brought on by an infection is referred to as an infectious disease, which is often known as a transmissible disease or communicable disease [3]. Many different pathogens can cause infections, but the bacteria are the most common causative agents that affect the host, as well as posing a risk of a major secondary infection [4]. Mammalian hosts respond to infections by first going through an innate response, which frequently involves inflammation, and then going through an adaptive response [5].

Herein, the treatment of microbial infections was carried out using antibiotics, antivirals, antifungals, antiprotozoals, and anthelmintics. Indeed, more than 9.2 million people died from infectious diseases in 2023, which means that more than 17% of all deaths were caused by infectious diseases, referring to the area of medicine that focuses on infections [6,7].

Unfortunately, antimicrobial agents are usually recorded as having dangerous side effects on normal cells, which means the specificity and selectivity of promising agents sometimes cannot be controlled. Therefore, the formulation of biological agents or drugs is

a recommended strategy not only to reduce those side effects, but also to improve the role and dosage design [8,9].

In this context, a bimetallic nanoparticle could overcome the multiresistance of microbial infections as well as cause a nice synergetic effect between the bimetallic metals that largely amplify the antimicrobial activity [10]. Various methods were used to synthesize nanoparticles that are listed as chemical, physical, and biological techniques [11]. The chemical method is not recommended due to environmental issues. However, the biological and physical methods are recognized as green processes for ZnONPs synthesis, whereas the biological method is still limited in terms of productivity [12]. Moreover, the in situ synthesis of bimetallic nanoparticles using physical methods is noted in the literature as excellent at meeting energy and equipment needs [13].

When employed as an adjuvant therapy to chemotherapy medications, zinc oxide nanoparticles (ZnONPs) can have a variety of therapeutic benefits, including antibacterial, anticancer, immunomodulatory, sunscreen, and antioxidant properties [14]. ZnONPs are extensively used as dermo-compatible and editable compounds, and also it is recommended as antimicrobial and anticancer agent with good cytocompatibility properties [15] and promising photoactivity that supports biological activity mechanism [16]. On the other hand, the use of Fe_3O_4 nanoparticles in several novel fields will be highlighted, including energy storage, biosensing, environmental applications for the removal of heavy metals and organic pollutants, moreover it is use in development of magnetic resonance imaging (MRI) contrast agents, as well as antimicrobial and anticancer drug delivery agents with a good biosafety profile [17,18]. Moreover, Fe_3O_4 nanoparticles are characterized by unique physicochemical properties, such as those of magnetic and electrical properties [19].

Indeed, ZnO@Fe_3O_4 NPs exhibit good antimicrobial activity that are relevant to the synergetic effect of the antimicrobial activity of both metals, which are induced by a higher free energy change, leading to the increased generation of the reactive oxygen species (ROS) [20,21]. Undoubtedly, bimetallic nanoparticles are an innovative notion that is acceptable due to their excellent multifunctionality that has been reported in the last few years [22–24]. In particular, the biocompatibility process plays an important role in the usability of bimetallic nanoparticles, and the formulation of bimetallic nanoparticles are usually recommended to enhance their stability and usability, while decreasing or eliminating the side effects as well [25].

Biopolymers are usually editable, compatible, and non-toxic because they are produced mainly by biological systems [26,27]. One of the biopolymers that can be separated from both human and animal milk is casein [28]. Evidently, this renders casein essentially non-toxic and compatible. In addition, casein is chemically characterized as a phosphoprotein that is chemically active and adaptable [29]. Additionally, one of the most significant edible biopolymers used globally is starch. The two forms of alpha-glucan polysaccharide that make up the majority (98–99%) of starch are amylose (-(1-4)) and amylopectin (-(1-6)) in granules made of glucose units [30]. Here, the bioactive nanocomposite that is decorated with nanometals could exhibit strong antimicrobial, anticancer, and antioxidant activities, all while maintaining biocompatibility [31–35].

Evidently, the chief disadvantages of prepared nanoparticles are their synthesis approach, their instability, and the cytotoxicity they cause due to their ability to be easily released. Furthermore, biocompatibility has a limited impact on whether the formulated materials will be accepted or rejected for biomedical applications, as incompatible materials can damage cells and tissues, resulting in destruction [36–38]. Therefore, the present work offers an eco-friendly approach to fabricate a completely biocompatible, antimicrobial, and antioxidant nanocomposite based on biopolymers like casein and starch encapsulated with ZnO@Fe_3O_4 NPs, which are synthesized in situ, with the biopolymers acting as capping and stabilizing agents. The prepared nanocomposite was characterized using advanced techniques to affirm the structure, including physiochemical and topographical analyses. Additionally, the biological profile will include antimicrobial, release, cytotoxicity, and antioxidant activities.

2. Materials and Methods

2.1. Materials

Soluble casein and starch were purchased from Sigma-Aldrich Co. (Darmstadt, Germany). Zinc acetate pentahydrate and ferric chloride were purchased from Loba Chem. Co. (Maharashtra, India). All microbial tissue culture media and reagents were purchased from Loba Chem. Co. (India) and were used as received.

2.2. Methodology

The formulation of ZNO@Fe_3O_4 NPs was carried out in situ during the preparation of nanocomposite-based biopolymers, namely, casein and starch, according to previous studies with minor modifications [39,40]. In detail, one gram of soluble casein was dissolved in 100 mL 1% acetic acid solution. Also, one gram of starch was dissolved in 100 mL of deionized water. Both solutions were individually and vigorously stirred at 1500 rpm at 70 °C for 2 h and mixed while stirring at 1500 rpm for 2 h till the solution became milky brown in color, that indicating the end point of this step. Afterward, the above-prepared solutions were ultrasonicated in an ultrasonic water bath at 70 °C for 2 h. In addition, zinc acetate and ferric chloride solutions were prepared separately with a concentration of 1% (*w*/*v*) in deionized water. The above three preprepared solutions were mixed (total volume 300 mL), whereas the metal salt solutions were added dropwise to avoid aggregation under vigorous stirring at 1500 rpm at 95 °C till the volume decreased to 200 mL. Finally, the collected solution was concentrated again to 100 mL, and then sonicated with an ultrasonic probe for 10 min. The preprepared nanocomposite was washed several times with 70% alcohol and centrifuged at 1000 rpm at least three times before lyophilization and preservation in a refrigerator for further investigations.

2.3. Characterizations

The characterizations of the prepared nanocomposite were carried out via physiochemical and morphological analyses and compared with those of neat materials. Physiochemical analysis involved an Ultraviolet–visible (UV-Visible) spectrophotometer (Jasco, V-630, Tokyo, Japan) in the range of 200–1000 nm, Fourier-transform infrared spectroscopy (FTIR) using an Impact-400 FT-IR spectrometer (Nicolet Analytical Instruments, 5225-1, Madison, WI, USA) in the range of 400–4000 cm^{-1}, and X-ray diffraction (XRD) at a 2θ (Bragg angle) of 5–80° using a Bruker D8 Advance X-ray diffractometer (Karlsruhe, Germany). Additionally, in this morphological study, transmission electron microscopy (TEM) was carried out using a high-resolution electron microscope (HRTEM, JEOL 2010, Tokyo, Japan) operating at 300 kV and selected area electron diffraction (SAED). Scanning electron microscope (SEM) images were taken using a scan electron microscope attached with EDX, Model Quanta 250 FEG (Field Emission Gun) attached to an EDX Unit (Energy Dispersive X-ray Analyses), and thermal stability analysis was carried out in a nitrogen atmosphere with a heating rate of 10 °C/min using an SDT Q600 thermal analyzer, TA Instruments, New Castle, DE, USA.

2.4. Biological Profile

The biological profile study was included a cytotoxicity assay, antimicrobial activity and antioxidant activity. The cytocompatibility test of the nanocomposite was carried out using the MTT protocol [41] with minor modifications against the human normal cell line, Wi 38, and Vero fibroblast normal cells were collected from the American type culture collection (ATCC). The cell quantity and the percentage of viable cells were calculated according to the following equation,

$$\text{Viability } \% = \frac{\text{Test OD}}{\text{Control OD}} \times 100$$

Additionally, the antimicrobial activity study was carried out using the turbidimetric assay, as carried out in our previous work [42], with an initial concentration of 100 µg/mL

nanocomposite. The microbes used in this study were Gram-positive (*Bacillus subtilis* ATCC 6051 and *Staphylococcus aureus* ATCC 25923), Gram-negative (*Escherichia coli* ATCC 25922 and *Pseudomonas aeruginosa* ATCC 27853), unicellular fungi (*Candida albicans* ATCC 90028), and filamentous fungi (*Aspergillus niger* RCMB 02724). The time required for the killing assay was calculated according to previous work, with minor modifications [43], as 24 h for bacteria and unicellular fungi and 72 h for filamentous fungi.

According to [44,45], the DPPH method was used for the antioxidant activity assessment, which was carried out according to the radical scavenging ability. To assess the antioxidant activity behavior of the extracted SNPs, the tested samples were generated in various concentrations with a range of 1–12%.

2.5. Statistical Analysis

The means of three replicates and standard errors were calculated for all obtained results, and the data were subjected to analysis of variance means using Minitab 21.2 software.

3. Results and Discussion

3.1. Formulation of Nanocomposite

The formulation of the nanocomposite was carried out based on casein and starch biopolymers used as capping and stabilizing agents for the green synthesis of ZNO@Fe_3O_4 NPs. The formulated nanocomposite was formulated in one step via a green methods, in which the reducing particle size and formulation was carried out.

3.2. Characterization of the Prepared Nanocomposite

The physicochemical analysis and topographical study were used to evaluate the properties of the nanocomposite, which is sometimes required to compare its neat materials. UV-vis spectroscopy was used to illustrate the performance of the nanoparticles via surface plasmon resonance adsorption peaks that are specific for each nanoparticle, especially metals and metal oxides. Figure 1a illustrates the UV-vis spectrum of the nanocomposite, where two bands were observed at 263 and 374 nm due to Fe_3O_4 NPs and ZnO NPs, respectively [46,47]. Obviously, the bands were presented broadly, which could be due to two reasons: the interaction between bimetallic structure and the entrance of bimetallic particles into the biopolymers helix, that affect the surface plasmon resonance. The TEM study reflected the size and arrangement of the nanoparticles, as shown in Figure 1b,c. The nanocomposite typically appeared as nanostructure that consisted of matrix containing bimetallic nanoparticles. Obviously, the matrix was assigned as a nanostructure that connected the bimetallic nanoparticles that had rod shapes arranged together as a strap. Moreover, these nanorods could be referred to as ZnONPs and Fe_3O_4NPs [48,49]. However, in regard to binding both metal oxide nanoparticles, the texture of bimetallic particles was recorded as a rough surface containing many scars that could be due to Fe_3O_4NPs' texture, and this observation agrees well with [50]. In this context, the SEAD pattern was observed as a polycrystalline behavior for the nanocomposite, with four rings arranged inside each other that could be as a result for interaction between the biopolymers and bimetallic nanoparticles [51]. In summary, the HR-TEM images emphasize the nanostructure of the nanocomposite, which agrees well with the UV-vis analysis conclusion. In this context, the bimetallic particles were recorded with the following dimensions: 85 nm long and 13 nm wide.

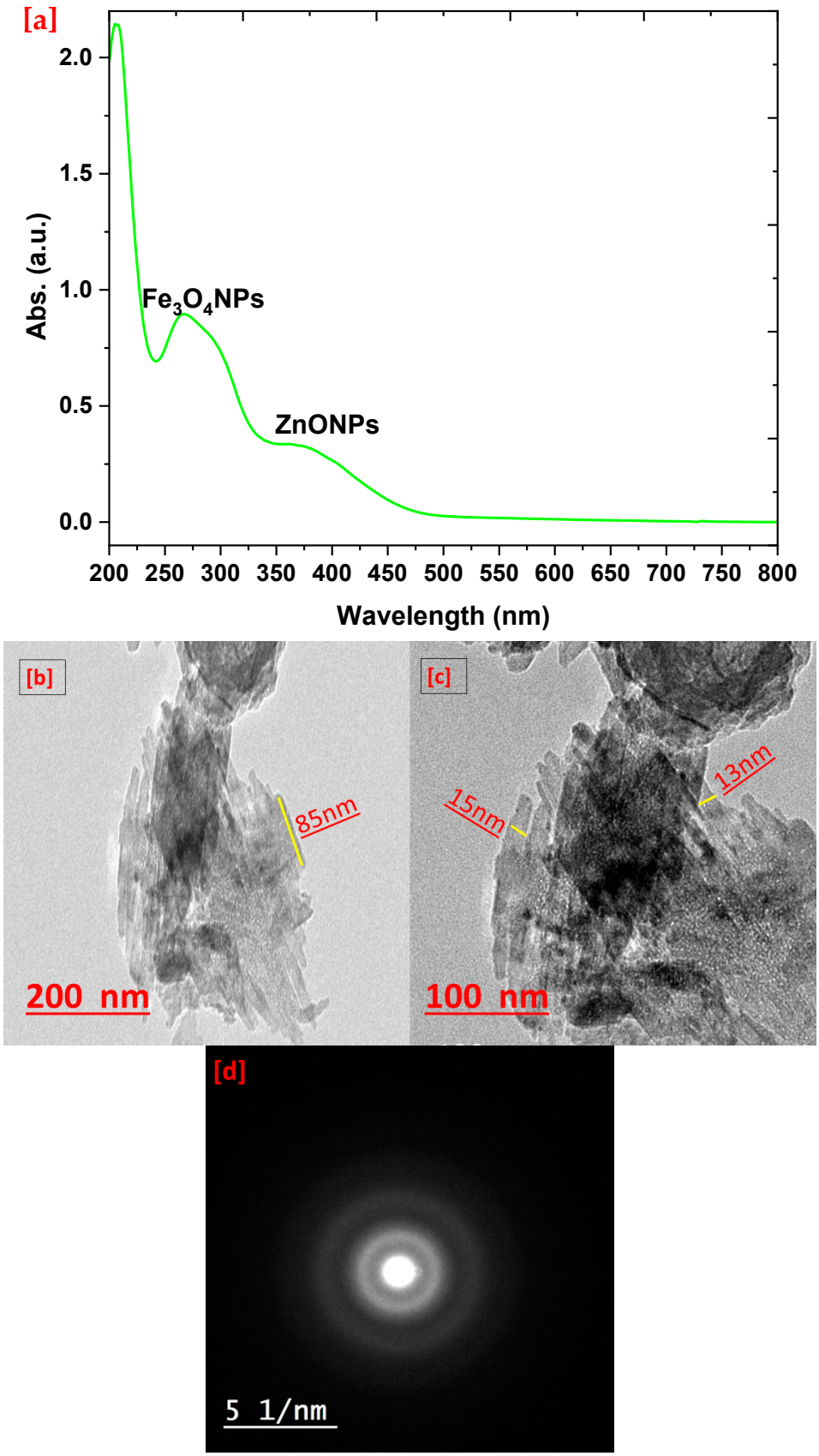

Figure 1. UV-vis of prepared nanocomposite (**a**) and HR-TEM images at low (**b**) and high (**c**) magnifications as well as the SEAD pattern (**d**).

FTIR spectroscopy was used to assign the function group changes and reactivity, as presented in Figure 2. The starch spectrum presented bands at 3290, 2925, 1635, 1420, 1340, 1008, 870, and 755 cm^{-1}, which are corresponding to the stretching vibrations of hydroxyl groups, CH_2 stretching, H-O-H bending, CH_2 bending, twisting of α-1,4 glycosidic linkage (C-O-C), C(1)-H deformation, CH_2 deformation, and C-C stretching, respectively [30,52,53]. Furthermore, the casein spectrum showed characteristic bands at 3281 and 3092 cm^{-1}, corresponding to the overlapping of amide A with hydroxyl group vibrations and amide B, respectively [54,55]. Additionally, the bands at 2956, 2915, and 2850 cm^{-1} were assigned to different C-H stretching and bending modes. The bands at 1635 and 1520 cm^{-1} are referred to as amide I, and a band at 1065 cm^{-1} for C-O-C of carboxylate compounds was recorded at 1446 cm^{-1} [54,56].

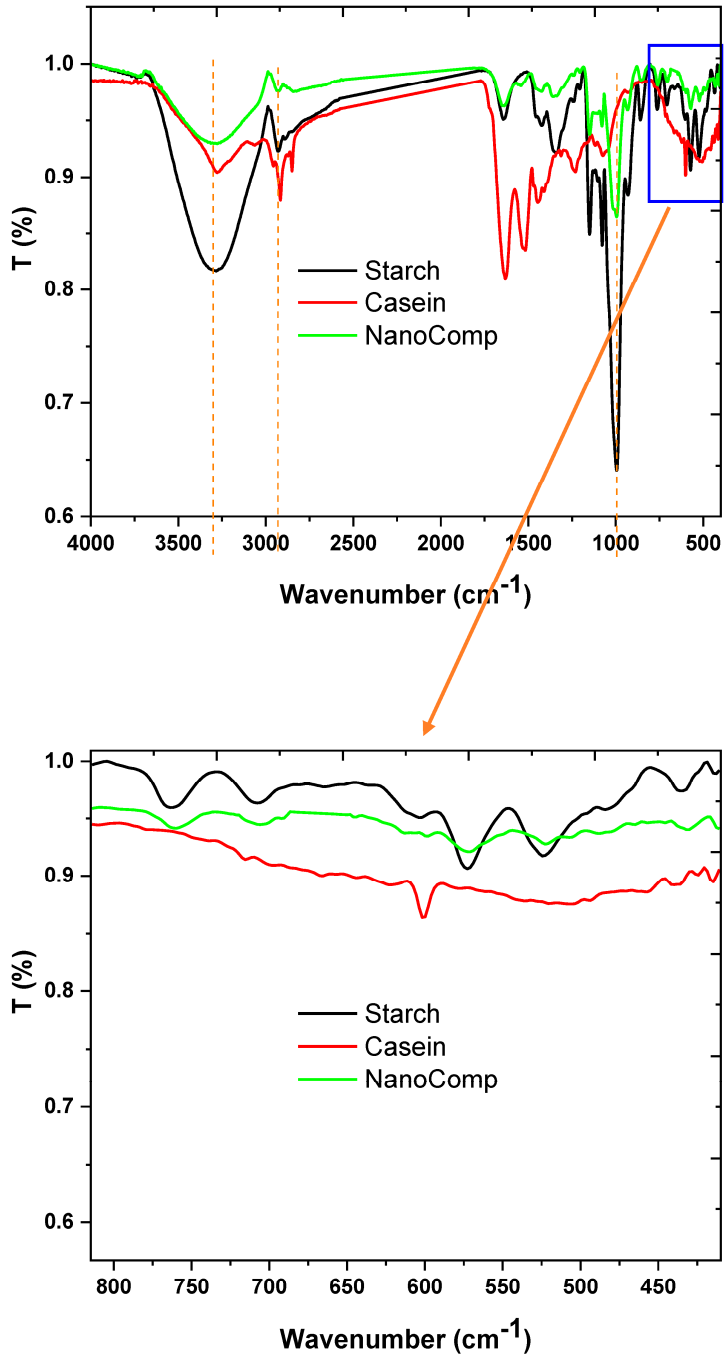

Figure 2. FTIR of nanocomposite and its neat materials.

On the other hand, the nanocomposite spectrum reflected more significant changes in comparison with those of its neat materials, not only in the bands' positions, but also in the bands' shape and intensity, which affirms the combination and excellent compatibility between the nanocomposite components at a molecular level. The band at 3290 cm^{-1} appeared as a result of the interaction between starch (-OH) and casein (-NH), which was broader than both, and the band of CH stretching was assigned to 2925 cm^{-1} as a small band. Moreover, the amide I band was shifted to a higher frequency, which may be due to the interaction between starch (-OH) and casein (-NH) that increases the negative charge around the amide group and increases the frequency as well. Additionally, the carbohydrate band was assigned at approximately at the same position, but with a low intensity. Moreover, the bimetallic nanoparticles were noted as small bands at 428 and 407 cm^{-1}, which referred to Zn-O [57], and Fe-O bands were recorded at 641 and 580 cm^{-1} [58], and the overlapped areas between both nanoparticles were noted as small bands at 690, 508, and 446 cm^{-1} [59]. Clearly, the FTIR study affirmed that the nanocomposite at the molecular level was prepared with new features that were different than those of its parent component.

The crystallographic analysis of the nanocomposite and its parent materials is presented in Figure 3. XRD was used to perform crystallography for the materials that were significantly changed after being doped with nanometal and nanometal oxides. The starch pattern referred to characteristic peaks at 2θ = 11. 15, 17, 19, 22, and 24° that related to native starch crystallography values [52,60,61]. The casein pattern was shown peaks at 2θ = 9 and 21°, where this peak and pattern behavior was typical with neat casein [62–64]. In addition, the nanocomposite pattern presented peaks that represented to the biopolymers interactions at 2θ = 13, 15, 19, 20, 23, and 25°, where these peaks noted in pattern of the pure starch and casein, whereas other peaks were noted at 2θ = 30, 32, 34, 36, 43, 47, 49, and 55° that were referred to the overlapping of ZnONPs and Fe_3O_4 [65–68]. Indeed, crystallographic analysis emphasized that the bimetallic nanoparticles well matched with the card number (JCPDS FILE No., 06–362) for ZnONPs [69] and (JCPDS98-0625) for Fe_2O_3 [46], with a minor difference that could be due to interactions between bimetallic particles as well as the formulation of the nanocomposite's new network, which may affect the molecular structure of the particles. These assumptions agree well with the UV-vis and FTIR studies' conclusions.

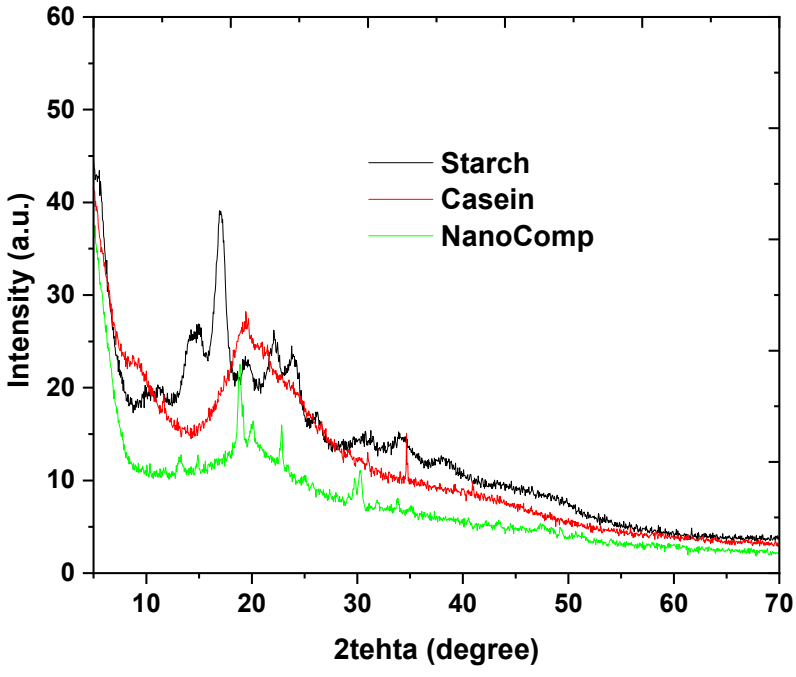

Figure 3. XRD patterns of nanocomposite and its neat materials.

Figure 4 presents SEM images of the nanocomposite and its neat components as well as the mapping and EDX chart of the nanocomposite. The SEM study reflects the surface behaviors, the EDX data present the elemental analysis of the samples, and the map affirms the elemental distribution. Figure 4a shows the native starch image that performed atypical morphology of pure starch with a unique spherical shape. Additionally, the casein surface (Figure 4b) appeared as a bulky structure, which is related to a conventional casein surface, with some pores that give the surface morphology a rough texture. In this context, the nanocomposite image at low magnification (Figure 4a) was observed as a smooth surface decorated with metal-like rods. However, the highly magnified image (Figure 4d) appeared a small rods collected together as a straps in a matrix, over which these rods could be collected or attached, contained holes. Herein, these observations affirm the TEM study conclusions as well. Nevertheless, the EDX chart (Figure 4g) shows the elemental analysis of the nanocomposite, which contains carbon, oxygen, nitrogen, sulfur, iron, and zinc. Furthermore, the mapping images of Zn and Fe in Figure 4e,f, respectively, were shown that the bimetallic particles offer an excellent distribution over the nanocomposite matrix.

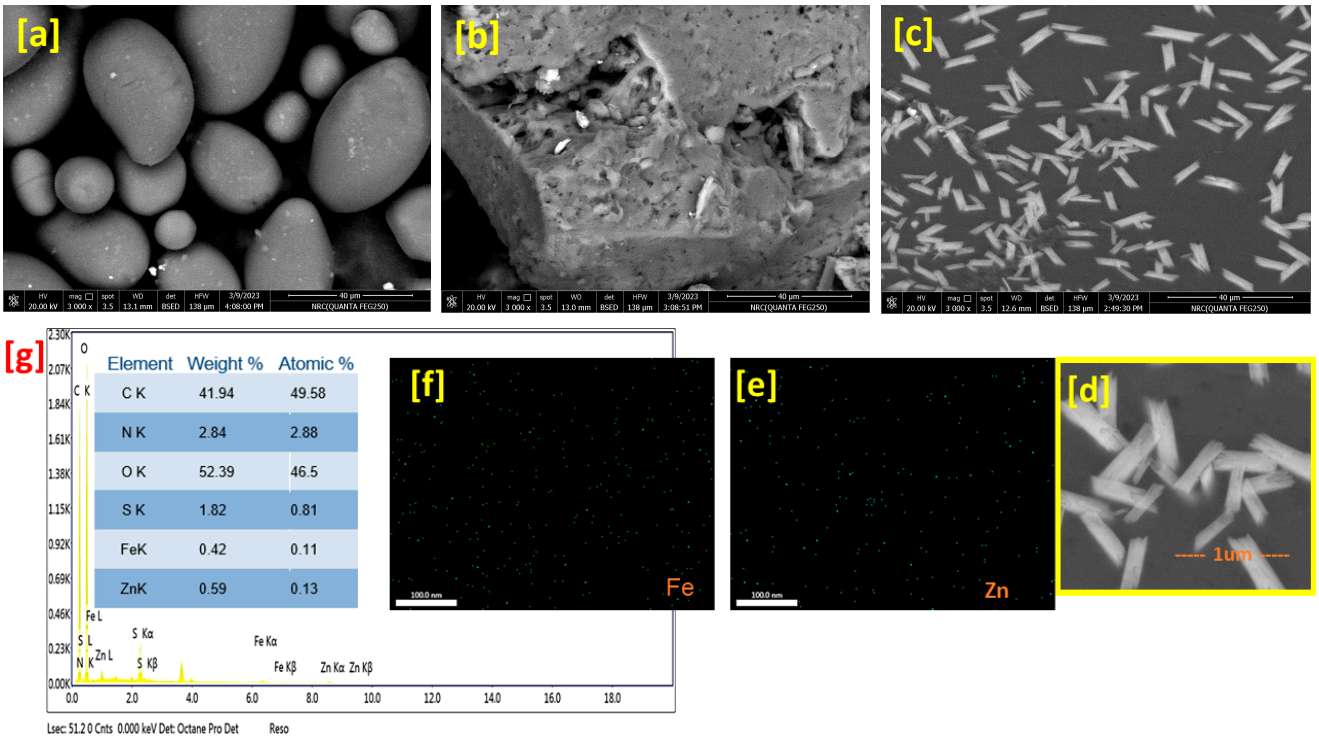

Figure 4. SEM images of neat starch (**a**), casein (**b**) and nanocomposite at low (**c**) and high (**d**) magnifications as well as mapping of Zn atom (**e**), Fe atom (**f**), and EDX chart (**g**).

The thermal behavior of the nanocomposite was studied using TGA and DTGA, and then was compared to its parent components, as presented in Figure 5. It is well known that thermal analysis studies not only refer to thermal stability, but also affirms the structure's stability. The TGA charts presented in Figure 5a, that presented a thermal stability of nanocomposite in comparison with its parent materials, as well as showed remaining weight refers to metal oxide nanoparticles. Otherwise, the decomposition of the nanocomposite was delayed in comparison with that of starch and casein. On the other hand, the DTGA data (Figure 5b) illustrate the main decomposition stage and the recorded peaks for starch, casein, and nanocomposite at 289, 303, and 345 °C, respectively. In this context, the stage of decomposition of pure starch started at 203 °C and ended at 416 °C, and for casein started at 238 °C and ended at 358 °C, whereas the nanocomposite recorded a starting decomposition temperature at 226 °C, that dropped, recovered, and then restarted

at 246 °C and ended at 529 °C. These observations, especially for the nanocomposite, were due to the reconfiguration of the molecular structure after it was imbedded with nanoparticles, so that, at first, small peaks adsorbed the temperature according to thermal conductivity and configurated with the polymer matrix, which affected the thermal stability positively [70,71].

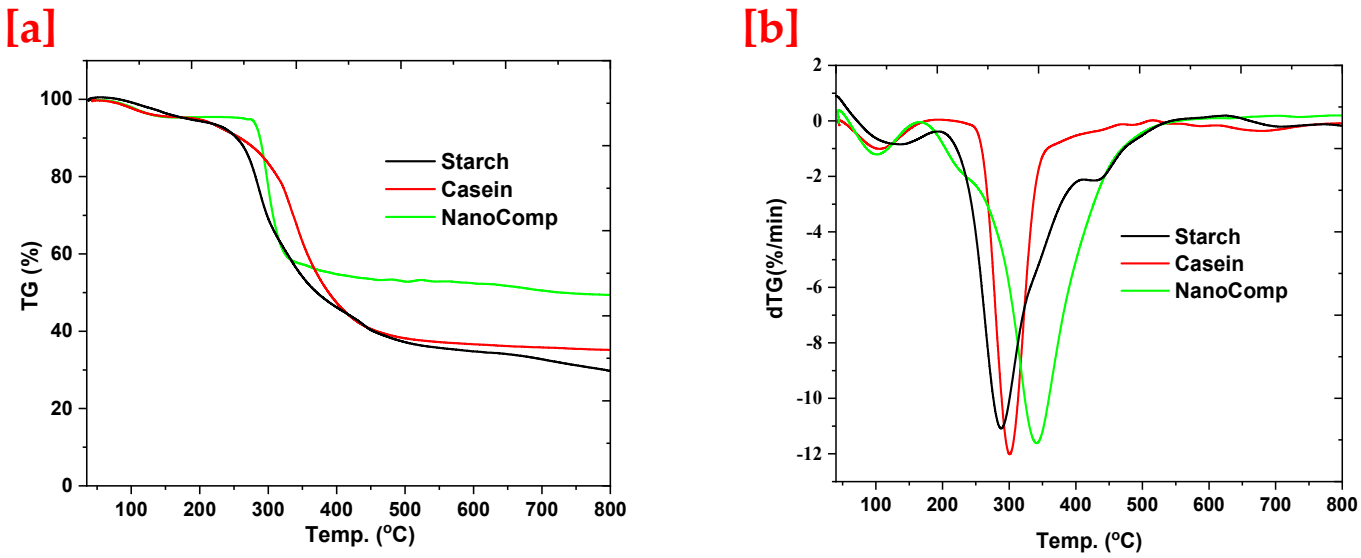

Figure 5. Thermal analysis of neat starch, casein, and nanocomposite TGA (**a**) and DTGA (**b**).

3.3. Biological Profile

The biological profile of the prepared nanocomposite was tested against microbial pathogens, including bacteria (Gram positive and negative) and fungi (unicellular and filamentous). Additionally, the biocompatibility property was tested using the Wi 38 human normal cell line and Vero fibroblast cell lines. Also, an antioxidant activity assay using DPPH was carried out to evaluate the complementary biological profile of the formulated nanocomposite.

3.3.1. Cytocompatibility Test

The cytocompatibility test was performed using the Wi 38 human normal cell line and Vero fibroblast cell lines, as presented in Figure 6. The produced nanocomposite demonstrated cytocompatibility up to 550 and 650 mg/mL for the Wi 38 and Vero cells, respectively, after exposure to concentrations of 100–1000 mg/mL. Moreover, the IC_{50} was 480 µg/mL for Wi 38, and that for the Vero cells were recorded as 450 mg/mL, which is regarded as having great cell compatibility. Furthermore, at high concentrations (greater than 500 mg/mL), the cell was healthy and did not exhibit any signs of significant deformation, shrinkage, or swelling. This indicates that the high concentration of the nanocomposite did not affect the cells directly, but rather the composition of the culture medium as a result of the adsorption of medium nutrients that affected a growth number of cells [72,73]. Overall, the obtained results affirmed that the prepared nanocomposite has high cytocompatibility, which means low cytotoxicity.

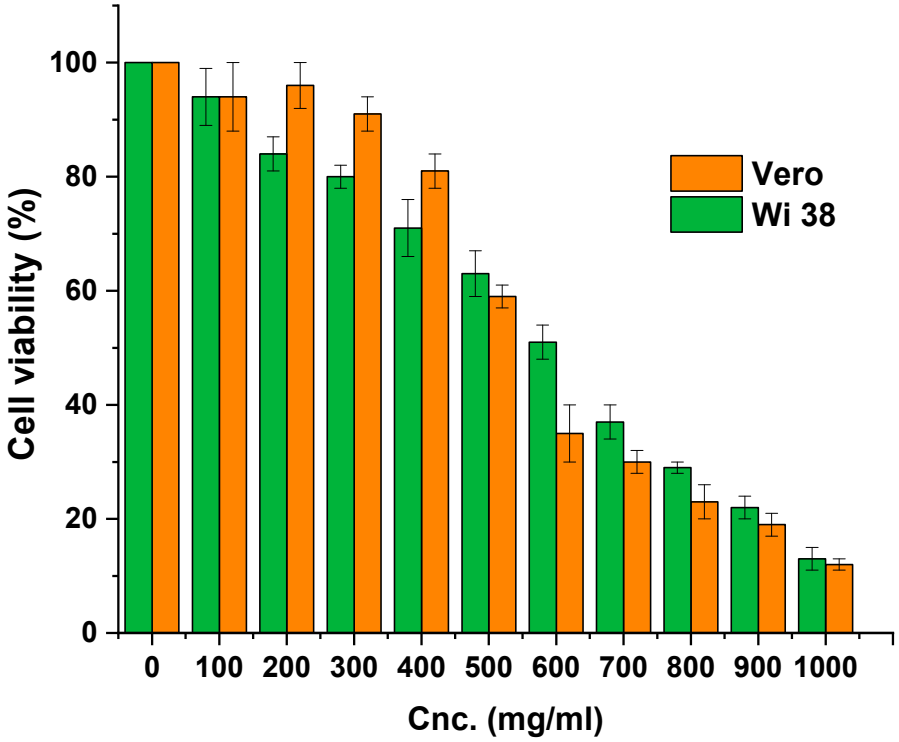

Figure 6. The cytocompatibility test was performed using the Wi 38 human normal cell line and Vero fibroblast cell lines against formulated nanocomposite.

3.3.2. Antimicrobial Activity Study

Six pathogenic microorganisms representing Gram-positive, Gram-negative, unicellular, and filamentous fungi were used in an antimicrobial investigation, as illustrated in Figure 7. Obviously, the formulated nanocomposite presented excellent antimicrobial activity against all the microbial populations recorded, such as 54% for filamentous fungi (Figure 7a). According to the mode of action, antimicrobial activity was gained from synergetic ZnO@Fe_3O_4, which has wonderful antibacterial activity that is pertinent to the synergetic impact of the antimicrobial activity of both metals, which is triggered by a larger free-energy change, leading to the increased formation of reactive oxygen species (ROS) [20,21,74]. Additionally, casein plays a role in antimicrobial activity via binding with the growth regulators of microbes as electrolytes and deactivating cell progression [75].

Moreover, the formulated nanocomposite was investigated to estimate the time required for killing and eradicating various microbial populations, as shown in Figure 7b. The killing rate of the bacterial strains was presented a slow rate during the first 5 h, thereafter the rate was faster, and the elimination of all Gram-negative bacterial cells after 16 h. Additionally, Gram-negative bacteria had a high death rate, but this occurred over a longer period than that of the positive ones. Furthermore, all bacterial strains had finished killing after 18 h, and this rate is regarded as high. In addition, the killing rate of unicellular fungi was detected as slower than that of bacteria, where the time needed to kill was found to be 19 h. However, the filamentous fungi showed the lowest rate of killing during the first 8 h, but the pace accelerated after 12 h, reaching a plateau. Since the rate of growth coincides with the death rate, the killing rate of filamentous fungi observed at 61 h was slower than that of unicellular fungi. Overall, it was discovered that the prepared nanocomposite had a promising death rate and efficacy against all microbiological populations.

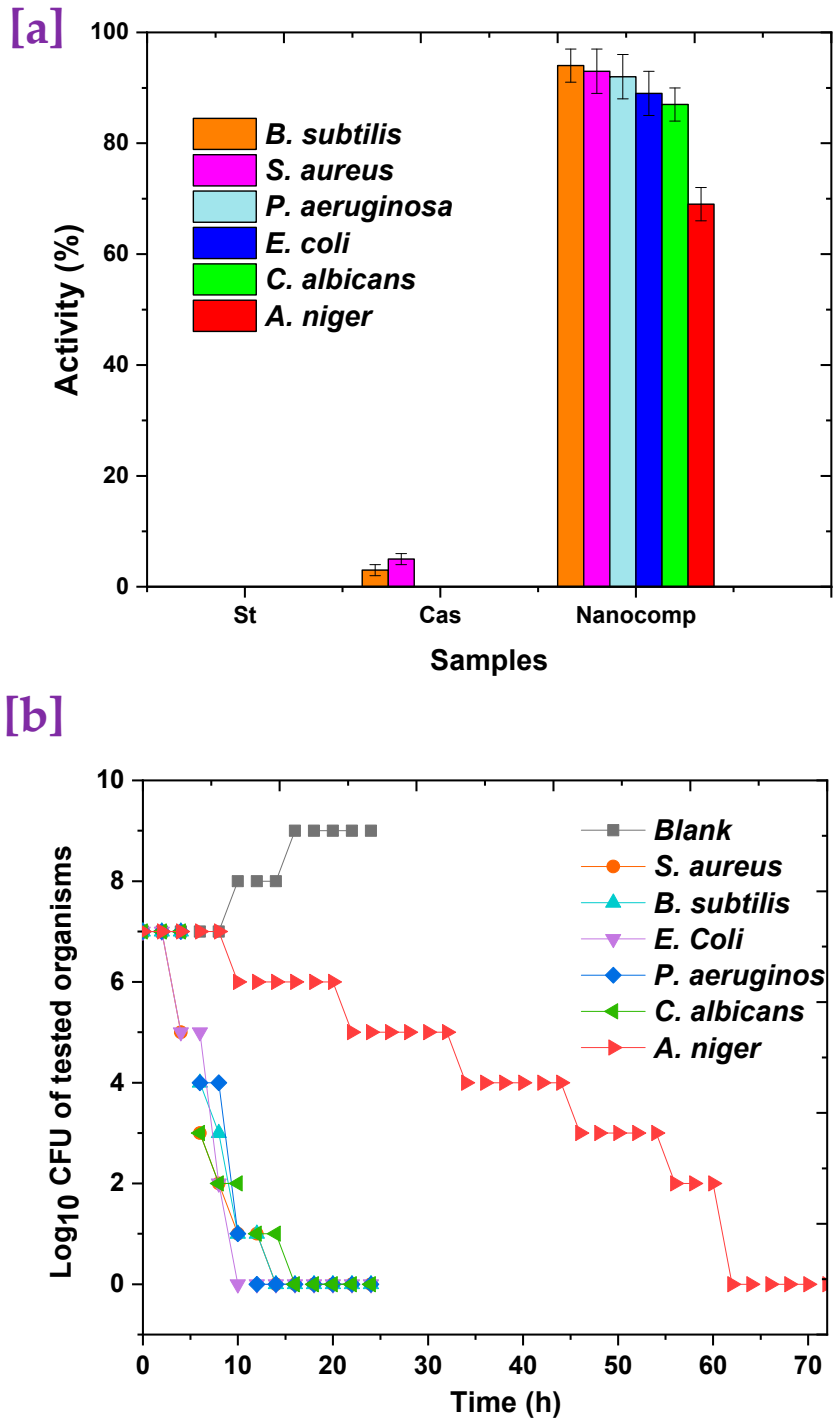

Figure 7. Antimicrobial study of formulated nanocomposite: (**a**) antimicrobial activity and (**b**) the time required for killing.

3.3.3. Antioxidant

The formulated nanocomposite underwent an antioxidant test to determine how well it functioned as an antioxidant substance. The antioxidant properties are shown in Figure 8 with different concentrations of the nanocomposite: 0–34% (*wt*/*v*). Consequently, the structure and the activity of the nanocomposite affected the DPPH reagent; the activity was reached 85% at concentrations of 28%. The obtained results highlight the antioxidant activity of the nanocomposite, which increases concurrently with the concentration of nanocomposite. Indeed, the antioxidant properties were gained from starch [30], casein [76],

and bimetallic nanoparticles [77,78] as well. Indeed, nanoparticles play a potential role in increasing the capacity of DPPH scavenging. Generally, the radicals generated during oxidation are a great way to combine the huge surface area of nanoparticles and reduce the oxidative activity of the free radicals [79]. In addition, starch has a role in inhibitory activity, thereby preventing the biochemical pathways that trigger the production of free radicals inside mitochondria [80]. Additionally, casein has a mechanism of antioxidant action, which forms a complex structure with free radicals and regulates their equilibrium to prevent oxidative reactions [81].

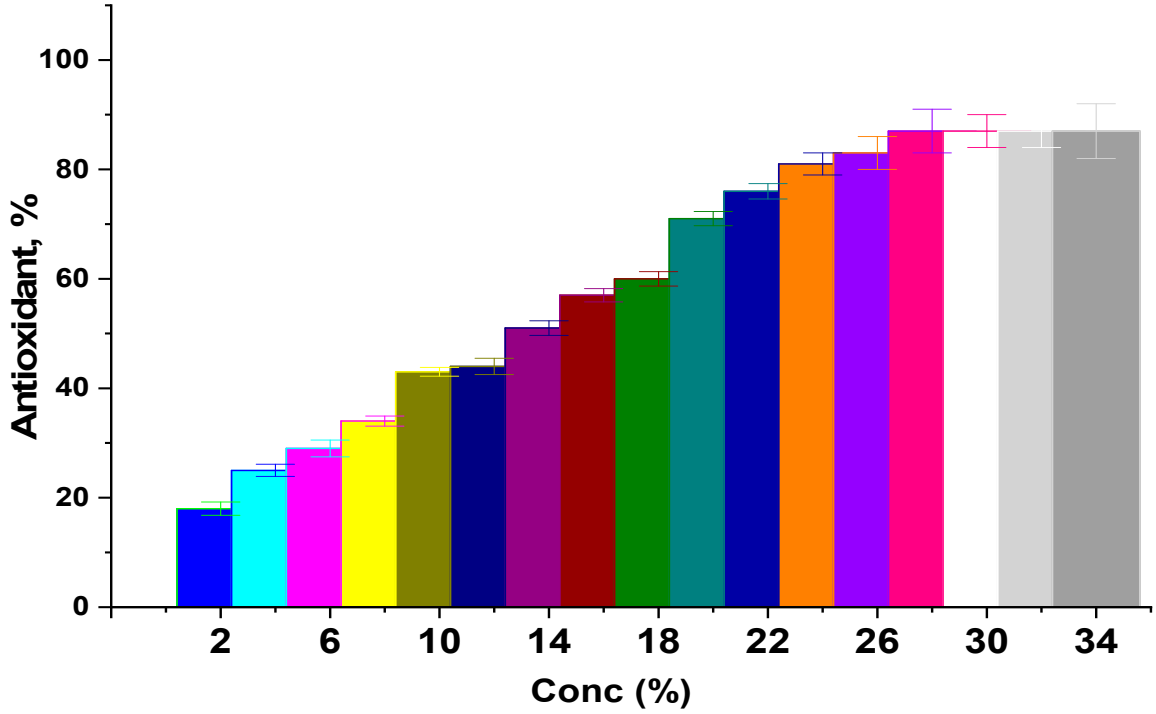

Figure 8. Antioxidant activity of formulated nanocomposite.

These outcomes not only highlight the antioxidant properties of the nanocomposite, but also support the effectiveness of the extraction technique, which preserve the distinctive characteristics of the generated nanocomposite.

4. Conclusions

The formulation of bimetallic nanoparticles into biopolymers was successfully achieved through a nanocomposite, according to physicochemical and topographical studies. Additionally, the formulated nanocomposite presented a nice cytocompatibility, with excellent IC50s as 550 and 650 mg/mL for Wi 38 and Vero cells, respectively, as well as a broad spectrum of antibacterial activity against Gram-positive and Gram-negative bacteria. Moreover, antifungal activity was assigned against unicellular and filamentous fungi, with a fast rate of killing. Antioxidant activity was observed at a concentration of 28% at about 85%. The formulated nanocomposite could be recommended to use as a multifunctional biologically active material for different biomedical applications.

Author Contributions: Conceptualization, A.S.A. and M.S.H.; Methodology, A.S.A., R.M.M. and M.S.H.; Software, R.M.M. and M.S.H.; Validation, A.S.A. and R.M.M. All authors have read and agreed to the published version of the manuscript.

Funding: This research was funded by University of Jeddah, Jeddah, Saudi Arabia grant number UJ-23-DR-93.

Institutional Review Board Statement: Not applicable.

Data Availability Statement: The datasets generated during and/or analyzed during the current study are available from the corresponding author upon reasonable request.

Acknowledgments: This work was funded by the University of Jeddah, Jeddah, Saudi Arabia, under grant No. (UJ-23-DR-93). Therefore, the authors thank the University of Jeddah for its technical and financial support.

Conflicts of Interest: The authors declare no conflict of interest.

References

1. Eisermann, I.; Garduño-Rosales, M.; Talbot, N.J. The emerging role of septins in fungal pathogenesis. *Cytoskeleton* **2023**. [CrossRef]
2. Salami, A.; Bettadapura, S.; Wang, S. Gasdermin D kills bacteria. *Microbiol. Res.* **2023**, *272*, 127383. [CrossRef]
3. Prabhu, S. Infectious and Communicable Diseases: An Overview. In *Textbook of General Pathology for Dental Students*; Springer: Cham, Switzerland, 2023; pp. 63–72.
4. Bansal, K.K.; Goyal, R.; Sharma, A.; Sharma, P.C.; Goyal, R.K. Repurposing of Drugs for the Treatment of Microbial Diseases. In *Drug Repurposing for Emerging Infectious Diseases and Cancer*; Springer: Berlin/Heidelberg, Germany, 2023; pp. 347–394.
5. Ortiz-Pérez, E.; Rivera, G.; Salas, C.O.; Zarate-Ramos, J.J.; Trofymchuk, O.S.; Hernandez-Soberanis, L.; Perales-Flores, J.D.; Vázquez, K. Natural and synthetic naphthoquinones as potential anti-infective agents. *Curr. Top. Med. Chem.* **2021**, *21*, 2046–2069. [CrossRef] [PubMed]
6. Cogo, M. The utilization of phytotherapy in place of traditional antibiotics to treat antimicrobial properties. *J. Clin. Immunol.* **2022**, *5*, 130.
7. Basappa, K.S.; Raghava, S.; Umesha, S. Potentials of Endophytic Fungus Untapped, including Novel Bioactive Compounds. *Pharmacogn. Commun.* **2023**, *13*, 50–63. [CrossRef]
8. Islam, F.; Shohag, S.; Uddin, M.J.; Islam, M.R.; Nafady, M.H.; Akter, A.; Mitra, S.; Roy, A.; Emran, T.B.; Cavalu, S. Exploring the journey of zinc oxide nanoparticles (ZnO-NPs) toward biomedical applications. *Materials* **2022**, *15*, 2160. [CrossRef] [PubMed]
9. Zhou, Z.; Li, B.; Liu, X.; Li, Z.; Zhu, S.; Liang, Y.; Cui, Z.; Wu, S. Recent progress in photocatalytic antibacterial. *ACS Appl. Bio Mater.* **2021**, *4*, 3909–3936. [CrossRef]
10. Hasanin, M.S.; Hashem, A.H.; Al-Askar, A.A.; Haponiuk, J.; Saied, E. A novel nanocomposite based on mycosynthesized bimetallic copper-zinc nanoparticles, nanocellulose and chitosan: Characterization, antimicrobial and photocatalytic activities. *Electron. J. Biotechnol.* **2023**, *65*, 45–55. [CrossRef]
11. Patil, N.; Bhaskar, R.; Vyavhare, V.; Dhadge, R.; Khaire, V.; Patil, Y. Overview on methods of synthesis of nanoparticles. *Int. J. Curr. Pharm. Res.* **2021**, *13*, 11–16. [CrossRef]
12. Faisal, S.; Jan, H.; Shah, S.A.; Shah, S.; Khan, A.; Akbar, M.T.; Rizwan, M.; Jan, F.; Wajidullah; Akhtar, N. Green synthesis of zinc oxide (ZnO) nanoparticles using aqueous fruit extracts of Myristica fragrans: Their characterizations and biological and environmental applications. *ACS Omega* **2021**, *6*, 9709–9722. [CrossRef]
13. Dou, S.; Xu, J.; Cui, X.; Liu, W.; Zhang, Z.; Deng, Y.; Hu, W.; Chen, Y. High-temperature shock enabled nanomanufacturing for energy-related applications. *Adv. Energy Mater.* **2020**, *10*, 2001331. [CrossRef]
14. Elshama, S.S.; Abdallah, M.E.; Abdel-Karim, R.I. Zinc oxide nanoparticles: Therapeutic benefits and toxicological hazards. *Open Nanomed. J.* **2018**, *5*, 16–22. [CrossRef]
15. Mohd Yusof, H.; Mohamad, R.; Zaidan, U.H.; Abdul Rahman, N.A. Microbial synthesis of zinc oxide nanoparticles and their potential application as an antimicrobial agent and a feed supplement in animal industry: A review. *J. Anim. Sci. Biotechnol.* **2019**, *10*, 57. [CrossRef]
16. Xia, G.; Zheng, Y.; Sun, Z.; Xia, S.; Ni, Z.; Yao, J. Fabrication of ZnAl-LDH mixed metal-oxide composites for photocatalytic degradation of 4-chlorophenol. *Environ. Sci. Pollut. Res.* **2022**, *29*, 39441–39450. [CrossRef]
17. Esmaeilzadeh, A.A.; Rasoolzadegan, S.; Arabi, A.R.; Soofi, D.; Rajaei Ramsheh, S.S.; Saad Ahmed, W.; Moaref Pour, R. Cytotoxic study of green synthesized pure and Ag-doped α-Fe_2O_3 nanoparticles on breast cancer (MCF-7) cell line. *Nanomed. Res. J.* **2022**, *7*, 370–377.
18. Shahrousvand, M.; Hoseinian, M.S.; Ghollasi, M.; Karbalaeimahdi, A.; Salimi, A.; Tabar, F.A. Flexible magnetic polyurethane/Fe_2O_3 nanoparticles as organic-inorganic nanocomposites for biomedical applications: Properties and cell behavior. *Mater. Sci. Eng. C* **2017**, *74*, 556–567. [CrossRef] [PubMed]
19. Sarani, M.; Hamidian, K.; Barani, M.; Adeli-Sardou, M.; Khonakdar, H.A. α-Fe_2O_3@ Ag and Fe_3O_4@ Ag Core-Shell Nanoparticles: Green Synthesis, Magnetic Properties and Cytotoxic Performance. *ChemistryOpen* **2023**, *12*, e202200250. [CrossRef] [PubMed]
20. Alangari, A.; Alqahtani, M.S.; Mateen, A.; Kalam, M.A.; Alshememry, A.; Ali, R.; Kazi, M.; AlGhamdi, K.M.; Syed, R. Iron oxide nanoparticles: Preparation, characterization, and assessment of antimicrobial and anticancer activity. *Adsorpt. Sci. Technol.* **2022**, *2022*, 1562051. [CrossRef]
21. Sardella, D.; Gatt, R.; Valdramidis, V.P. Physiological effects and mode of action of ZnO nanoparticles against postharvest fungal contaminants. *Food Res. Int.* **2017**, *101*, 274–279. [CrossRef]
22. El-Shishtawy, R.M.; Ahmed, N.S.; Almulaiky, Y.Q. Immobilization of catalase on chitosan/ZnO and chitosan/ZnO/Fe_2O_3 nanocomposites: A comparative study. *Catalysts* **2021**, *11*, 820. [CrossRef]

23. Alahabadi, A.; Shomoossi, N.; Riahimanesh, F.; Salari, M. Development of AC/ZnO/Fe_2O_3 for efficiently adsorptive removal of Tetracycline from water environment: Isotherm, kinetic and thermodynamic studies and adsorption mechanism. *Biomass Convers. Biorefinery* **2023**. [CrossRef]
24. Lu, J.; Shan, X.; Wu, Q.; Zhao, Y.; Li, C.; Li, H.; Yang, S.; Tian, L. ZnO-Fe_2O_3 based electrochemiluminescence sensor for sensitive detection of malathion. *Microchem. J.* **2023**, *186*, 108321. [CrossRef]
25. Shehabeldine, A.; El-Hamshary, H.; Hasanin, M.; El-Faham, A.; Al-Sahly, M. Enhancing the antifungal activity of griseofulvin by incorporation a green biopolymer-based nanocomposite. *Polymers* **2021**, *13*, 542. [CrossRef] [PubMed]
26. Abdelraof, M.; Ibrahim, S.; Selim, M.; Hasanin, M. Immobilization of L-methionine γ-lyase on different cellulosic materials and its potential application in green-selective synthesis of volatile sulfur compounds. *J. Environ. Chem. Eng.* **2020**, *8*, 103870. [CrossRef]
27. Hasanin, M.S. Cellulose-Based Biomaterials: Chemistry and Biomedical Applications. *Starch-Stärke* **2022**, *74*, 2200060. [CrossRef]
28. de Kruif, C.G.; Huppertz, T.; Urban, V.S.; Petukhov, A.V. Casein micelles and their internal structure. *Adv. Colloid Interface Sci.* **2012**, *171–172*, 36–52. [CrossRef]
29. Delom, F.; Chevet, E. Phosphoprotein analysis: From proteins to proteomes. *Proteome Sci.* **2006**, *4*, 15. [CrossRef]
30. Hasanin, M.S. Simple, economic, ecofriendly method to extract starch nanoparticles from potato peel waste for biological applications. *Starch-Stärke* **2021**, *73*, 2100055. [CrossRef]
31. Agarwal, A.; Rizwana; Tripathi, A.D.; Kumar, T.; Sharma, K.P.; Patel, S.K.S. Nutritional and Functional New Perspectives and Potential Health Benefits of Quinoa and Chia Seeds. *Antioxidants* **2023**, *12*, 1413. [CrossRef]
32. Valgimigli, L.; Baschieri, A.; Amorati, R. Antioxidant activity of nanomaterials. *J. Mater. Chem. B* **2018**, *6*, 2036–2051. [CrossRef]
33. Hasanin, M.S.; Youssef, A.M. Ecofriendly bioactive film doped CuO nanoparticles based biopolymers and reinforced by enzymatically modified nanocellulose fibers for active packaging applications. *Food Packag. Shelf Life* **2022**, *34*, 100979. [CrossRef]
34. Joseph, T.M.; Kar Mahapatra, D.; Esmaeili, A.; Piszczyk, Ł.; Hasanin, M.S.; Kattali, M.; Haponiuk, J.; Thomas, S. Nanoparticles: Taking a unique position in medicine. *Nanomaterials* **2023**, *13*, 574. [CrossRef] [PubMed]
35. Cao, W.; Hench, L.L. Bioactive materials. *Ceram. Int.* **1996**, *22*, 493–507. [CrossRef]
36. Manam, N.; Harun, W.; Shri, D.; Ghani, S.; Kurniawan, T.; Ismail, M.H.; Ibrahim, M. Study of corrosion in biocompatible metals for implants: A review. *J. Alloys Compd.* **2017**, *701*, 698–715. [CrossRef]
37. Reddy, M.S.B.; Ponnamma, D.; Choudhary, R.; Sadasivuni, K.K. A comparative review of natural and synthetic biopolymer composite scaffolds. *Polymers* **2021**, *13*, 1105. [CrossRef]
38. Wang, Y.; Xu, X.; Chen, X.; Li, J. Multifunctional biomedical materials derived from biological membranes. *Adv. Mater.* **2022**, *34*, 2107406. [CrossRef] [PubMed]
39. Gouda, M.; Al-Bokheet, W.; Al-Omair, M. In-situ deposition of metal oxides nanoparticles in cellulose derivative and its utilization for wastewater disinfection. *Polymers* **2020**, *12*, 1834. [CrossRef] [PubMed]
40. Ali, O.M.; Hasanin, M.S.; Suleiman, W.B.; Helal, E.E.-H.; Hashem, A.H. Green biosynthesis of titanium dioxide quantum dots using watermelon peel waste: Antimicrobial, antioxidant, and anticancer activities. *Biomass Convers. Biorefinery* **2022**. [CrossRef]
41. Grela, E.; Kozłowska, J.; Grabowiecka, A. Current methodology of MTT assay in bacteria—A review. *Acta Histochem.* **2018**, *120*, 303–311. [CrossRef] [PubMed]
42. Ibrahim, N.A.; Hasanin, M.S.; Kamel, S. A new approach for improving the antimicrobial activity of cellulose pulp. *Inorg. Chem. Commun.* **2023**, *155*, 111009. [CrossRef]
43. Balouiri, M.; Sadiki, M.; Ibnsouda, S.K. Methods for in vitro evaluating antimicrobial activity: A review. *J. Pharm. Anal.* **2016**, *6*, 71–79. [CrossRef]
44. Noreen, H.; Semmar, N.; Farman, M.; McCullagh, J.S. Measurement of total phenolic content and antioxidant activity of aerial parts of medicinal plant Coronopus didymus. *Asian Pac. J. Trop. Med.* **2017**, *10*, 792–801. [CrossRef]
45. Ibrahim, S.; Elsayed, H.; Hasanin, M. Biodegradable, Antimicrobial and Antioxidant Biofilm for Active Packaging Based on Extracted Gelatin and Lignocelluloses Biowastes. *J. Polym. Environ.* **2021**, *29*, 472–482. [CrossRef]
46. Takai, Z.I.; Mustafa, M.K.; Asman, S.; Sekak, K.A. Preparation and characterization of magnetite (Fe_3O_4) nanoparticles by sol-gel method. *Int. J. Nanoelectron. Mater* **2019**, *12*, 37–46.
47. Pudukudy, M.; Yaakob, Z. Facile Synthesis of Quasi Spherical ZnO Nanoparticles with Excellent Photocatalytic Activity. *J. Clust. Sci.* **2015**, *26*, 1187–1201. [CrossRef]
48. Pacheri Madathil, A.; Vanaja, K.; Jayaraj, M. Synthesis of ZnO nanoparticles by hydrothermal method. In *Nanophotonic Materials IV, Proceedings of the NANOSCIENCE + ENGINEERING, San Diego, CA, USA, 26–30 August 2007*; SPIE: Bellingham, WA, USA, 2007; Volume 6639, p. 6639.
49. Cao, D.; Shu, X.; Zhu, D.; Liang, S.; Hasan, M.; Gong, S. Lipid-coated ZnO nanoparticles synthesis, characterization and cytotoxicity studies in cancer cell. *Nano Converg.* **2020**, *7*, 14. [CrossRef] [PubMed]
50. Hu, H.; Yang, H.; Huang, P.; Cui, D.; Peng, Y.; Zhang, J.; Lu, F.; Lian, J.; Shi, D. Unique role of ionic liquid in microwave-assisted synthesis of monodisperse magnetite nanoparticles. *Chem. Commun.* **2010**, *46*, 3866–3868. [CrossRef]
51. De Graef, M. *Introduction to Conventional Transmission Electron Microscopy*; Cambridge University Press: Cambridge, UK, 2003. [CrossRef]
52. Warren, F.J.; Gidley, M.J.; Flanagan, B.M. Infrared spectroscopy as a tool to characterise starch ordered structure—A joint FTIR–ATR, NMR, XRD and DSC study. *Carbohydr. Polym.* **2016**, *139*, 35–42. [CrossRef]

53. Shivaraju, V.K.; Vallayil Appukuttan, S.; Kumar, S. The Influence of Bound Water on the FTIR Characteristics of Starch and Starch Nanocrystals Obtained from Selected Natural Sources. *Starch-Stärke* **2019**, *71*, 1700026. [CrossRef]
54. Singh, A.; Bajpai, J.; Tiwari, A.; Bajpai, A.K. Designing casein-coated iron oxide nanostructures (CCIONPs) as superparamagnetic core–shell carriers for magnetic drug targeting. *Prog. Biomater.* **2015**, *4*, 39–53. [CrossRef]
55. Szyk-Warszyńska, L.; Raszka, K.; Warszyński, P. Interactions of casein and polypeptides in multilayer films studied by FTIR and molecular dynamics. *Polymers* **2019**, *11*, 920. [CrossRef] [PubMed]
56. Wang, J.; Su, Y.; Jia, F.; Jin, H. Characterization of casein hydrolysates derived from enzymatic hydrolysis. *Chem. Cent. J.* **2013**, *7*, 62. [CrossRef] [PubMed]
57. Nagaraju, G.; Udayabhanu; Shivaraj; Prashanth, S.A.; Shastri, M.; Yathish, K.V.; Anupama, C.; Rangappa, D. Electrochemical heavy metal detection, photocatalytic, photoluminescence, biodiesel production and antibacterial activities of Ag–ZnO nanomaterial. *Mater. Res. Bull.* **2017**, *94*, 54–63. [CrossRef]
58. Nalbandian, L.; Patrikiadou, E.; Zaspalis, V.; Patrikidou, A.; Hatzidaki, E.; N Papandreou, C. Magnetic nanoparticles in medical diagnostic applications: Synthesis, characterization and proteins conjugation. *Curr. Nanosci.* **2016**, *12*, 455–468. [CrossRef]
59. Ulya, H.N.; Taufiq, A. Comparative structural properties of nanosized ZnO/Fe_3O_4 composites prepared by sonochemical and Sol-Gel methods. *IOP Conf. Ser. Earth Environ. Sci.* **2019**, *276*, 012059. [CrossRef]
60. Todica, M.; Nagy, E.M.; Niculaescu, C.; Stan, O.; Cioica, N.; Pop, C.V. XRD Investigation of Some Thermal Degraded Starch Based Materials. *J. Spectrosc.* **2016**, *2016*, 9605312. [CrossRef]
61. Pozo, C.; Rodríguez-Llamazares, S.; Bouza, R.; Barral, L.; Castaño, J.; Müller, N.; Restrepo, I. Study of the structural order of native starch granules using combined FTIR and XRD analysis. *J. Polym. Res.* **2018**, *25*, 266. [CrossRef]
62. Heep, G.; Almeida, A.; Marcano, R.; Vieira, D.; Mainardes, R.M.; Khalil, N.M.; Sarmento, B. Zein-casein-lysine multicomposite nanoparticles are effective in modulate the intestinal permeability of ferulic acid. *Int. J. Biol. Macromol.* **2019**, *138*, 244–251. [CrossRef]
63. Wu, X.; Liu, Q.; Luo, Y.; Murad, M.S.; Zhu, L.; Mu, G. Improved packing performance and structure-stability of casein edible films by dielectric barrier discharges (DBD) cold plasma. *Food Packag. Shelf Life* **2020**, *24*, 100471. [CrossRef]
64. Bhatia, S.; Al-Harrasi, A.; Al-Azri, M.S.; Ullah, S.; Bekhit, A.E.-D.A.; Pratap-Singh, A.; Chatli, M.K.; Anwer, M.K.; Aldawsari, M.F. Preparation and Physiochemical Characterization of Bitter Orange Oil Loaded Sodium Alginate and Casein Based Edible Films. *Polymers* **2022**, *14*, 3855. [CrossRef]
65. El-Belely, E.F.; Farag, M.M.; Said, H.A.; Amin, A.S.; Azab, E.; Gobouri, A.A.; Fouda, A. Green synthesis of zinc oxide nanoparticles (ZnO-NPs) using Arthrospira platensis (Class: Cyanophyceae) and evaluation of their biomedical activities. *Nanomaterials* **2021**, *11*, 95. [CrossRef]
66. Lingaraju, K.; Naika, H.R.; Nagabhushana, H.; Nagaraju, G. *Euphorbia heterophylla* (L.) mediated fabrication of ZnO NPs: Characterization and evaluation of antibacterial and anticancer properties. *Biocatal. Agric. Biotechnol.* **2019**, *18*, 100894. [CrossRef]
67. Muhammad, W.; Ullah, N.; Haroon, M.; Abbasi, B.H. Optical, morphological and biological analysis of zinc oxide nanoparticles (ZnO NPs) using *Papaver somniferum* L. *RSC Adv.* **2019**, *9*, 29541–29548. [CrossRef] [PubMed]
68. Rahmawati, R.; Permana, M.G.; Harison, B.; Nugraha; Yuliarto, B.; Suyatman; Kurniadi, D. Optimization of Frequency and Stirring Rate for Synthesis of Magnetite (Fe_3O_4) Nanoparticles by Using Coprecipitation- Ultrasonic Irradiation Methods. *Procedia Eng.* **2017**, *170*, 55–59. [CrossRef]
69. Elsayed, N.; Hasanin, M.S.; Abdelraof, M. Utilization of olive leaves extract coating incorporated with zinc/selenium oxide nanocomposite to improve the postharvest quality of green beans pods. *Bioact. Carbohydr. Diet. Fibre* **2022**, *28*, 100333. [CrossRef]
70. Bikiaris, D. Can nanoparticles really enhance thermal stability of polymers? Part II: An overview on thermal decomposition of polycondensation polymers. *Thermochim. Acta* **2011**, *523*, 25–45. [CrossRef]
71. Domínguez-Díaz, M.; Meneses-Acosta, A.; Romo-Uribe, A.; Peña, C.; Segura, D.; Espin, G. Thermo-mechanical properties, microstructure and biocompatibility in poly-β-hydroxybutyrates (PHB) produced by OP and OPN strains of Azotobacter vinelandii. *Eur. Polym. J.* **2015**, *63*, 101–112. [CrossRef]
72. Khan, I.; Saeed, K.; Khan, I. Nanoparticles: Properties, applications and toxicities. *Arab. J. Chem.* **2019**, *12*, 908–931. [CrossRef]
73. Gudkov, S.V.; Simakin, A.V.; Sarimov, R.M.; Kurilov, A.D.; Chausov, D.N. Novel Biocompatible with Animal Cells Composite Material Based on Organosilicon Polymers and Fullerenes with Light-Induced Bacteriostatic Properties. *Nanomaterials* **2021**, *11*, 2804. [CrossRef]
74. Fahim, A.M.; Hasanin, M.; Habib, I.; El-Attar, R.O.; Dacrory, S. Synthesis, antimicrobial activity, theoretical investigation, and electrochemical studies of cellulosic metal complexes. *J. Iran. Chem. Soc.* **2023**, *20*, 1699–1718. [CrossRef]
75. Singh, A.; Duche, R.T.; Wandhare, A.G.; Sian, J.K.; Singh, B.P.; Sihag, M.K.; Singh, K.S.; Sangwan, V.; Talan, S.; Panwar, H. Milk-Derived Antimicrobial Peptides: Overview, Applications, and Future Perspectives. *Probiotics Antimicrob. Proteins* **2023**, *15*, 44–62. [CrossRef]
76. Kim, Y.E.; Kim, J.W.; Cheon, S.; Nam, M.S.; Kim, K.K. Alpha-Casein and beta-lactoglobulin from cow milk exhibit antioxidant activity: A plausible link to antiaging effects. *J. Food Sci.* **2019**, *84*, 3083–3090. [CrossRef] [PubMed]
77. García-López, J.I.; Zavala-García, F.; Olivares-Sáenz, E.; Lira-Saldívar, R.H.; Díaz Barriga-Castro, E.; Ruiz-Torres, N.A.; Ramos-Cortez, E.; Vázquez-Alvarado, R.; Niño-Medina, G. Zinc oxide nanoparticles boosts phenolic compounds and antioxidant activity of *Capsicum annuum* L. during germination. *Agronomy* **2018**, *8*, 215. [CrossRef]

78. Feng, Y.; Kreslavski, V.D.; Shmarev, A.N.; Ivanov, A.A.; Zharmukhamedov, S.K.; Kosobryukhov, A.; Yu, M.; Allakhverdiev, S.I.; Shabala, S. Effects of iron oxide nanoparticles (Fe_3O_4) on growth, photosynthesis, antioxidant activity and distribution of mineral elements in wheat (*Triticum aestivum*) Plants. *Plants* **2022**, *11*, 1894. [CrossRef] [PubMed]
79. Ge, X.; Cao, Z.; Chu, L. The Antioxidant Effect of the Metal and Metal-Oxide Nanoparticles. *Antioxidants* **2022**, *11*, 791. [CrossRef]
80. Jayawardena, N.; Watawana, M.I.; Jayathilaka, R.T.; Waisundara, V.Y. The Antioxidant and Starch Hydrolase Inhibitory Activity of Ten Spices in an In Vitro Model of Digestion: Bioaccessibility of Anthocyanins and Carotenoids. *Evid.-Based Complement Altern. Med.* **2015**, *2015*, 764238. [CrossRef]
81. Cervato, G.; Cazzola, R.; Cestaro, B. Studies on the antioxidant activity of milk caseins. *Int. J. Food Sci. Nutr.* **1999**, *50*, 291–296. [CrossRef] [PubMed]